Investigations of femtosecond–nanosecond dual-beam laser ablation of dielectrics

Cheng-Hsiang Lin,[1,2] Zheng-Hua Rao,[2] Lan Jiang,[3] Wu-Jung Tsai,[4] Ping-Han Wu,[4] Chih-Wei Chien,[4] Shean-Jen Chen,[1] and Hai-Lung Tsai[2,*]

[1]*Department of Engineering Science, National Cheng Kung University, Tainan 701, Taiwan*

[2]*Department of Mechanical and Aerospace Engineering, Missouri University of Science and Technology, Rolla, Missouri 65409, USA*

[3]*Department of Mechanical and Automation Engineering, 3rd School, Beijing Institute of Technology, Beijing, 100081, China*

[4]*Laser Application Technology Center, ITRI South, Industrial Technology Research Institute, Tainan 73445, Taiwan*

**Corresponding author: tsai@mst.edu*

Received April 7, 2010; revised June 19, 2010; accepted June 25, 2010;
posted July 2, 2010 (Doc. ID 126686); published July 15, 2010

We have conducted experimental investigations for the micromachining of dielectrics (fused silica) using an integrated femtosecond (fs) and nanosecond (ns) dual-beam laser system at different time delays between the fs and ns pulses. We found that the maximum ablation enhancement occurs when the fs pulse is shot near the peak of the ns pulse envelope. Enhancements up to 13.4 times in ablation depth and 50.7 times in the amount of material removal were obtained, as compared to fs laser ablation alone. The fs pulse increases the free electron density and changes the optical properties of fused silica to have metallic characteristics, which increases the absorption of the ns laser energy. This study provides an opportunity for efficient micromachining of dielectrics. © 2010 Optical Society of America

OCIS codes: 140.3390, 140.7090.

The mechanism of material removal and the associated physical phenomena occurring during laser–matter interaction strongly depend on laser pulse duration. A femtosecond (fs) laser pulse can fully ionize almost any solid material with reduced recast, microcracks, and heat-affected zone. Hence, fs lasers are promising tools for the micro-/nanoscale fabrication of all types of materials [1–7], especially for wide-bandgap materials, due to the multiphoton effects. However, the throughput of fs lasers is too low to satisfy industrial demands. On the other hand, although nanosecond (ns) lasers have been popularly used in industry for processing metals, they cannot process dielectric materials.

Recently, the use of multibeam/multicolor lasers has attracted much attention in the field of laser micromachining. Sugioka *et al.* improved the machining quality and efficiency of fused quartz through the simultaneous irradiation of multiwavelength beams emitted from a vacuum-ultraviolet Raman laser whose short wavelength components increased the absorption of the fundamental beam at a 266 nm wavelength by photodissociation of Si—O bonds and the excited-state absorption [8]. Zhang *et al.* proposed the use of KrF excimer and F_2 laser multiwavelength excitation to reduce debris deposition and to improve ablation quality [9]. Although both fs–fs [10,11] and ns–ns [12] dual-pulse machining systems have been proposed, they encounter the same problems of low throughput for a fs–fs system and can process only nondielectric materials for a ns–ns system. In this study, an integrated fs–ns dual-beam machining system is proposed, aiming at the enhancement of material removal rate for dielectrics.

The fs–ns dual-beam laser micromachining system consists of a Ti:sapphire fs laser (Legend-F, Coherent), a diode-pump solid-state ns laser (AVIA-X, Coherent), a three-axis motion stage, and an imaging system for monitoring the machining process. The central wavelength and pulse duration for the fs laser are 800 nm and 120 fs, respectively, and are 355 nm and 30 ns, respectively, for the ns laser. The theoretical spot diameters of the fs and ns laser beams on the sample surface are, respectively, 1.85 μm and 0.86 μm. Both laser beams are in Gaussian distribution. As shown in the schematic diagram of Fig. 1, each of the fs pulses and ns pulses first passes through a combination of a half-wave plate and a linear polarizer to adjust the pulse energy. Then, both laser beams are combined into the same optical path via a long-pass dichroic mirror (DM1), which reflects ns laser pulses but allows the pass of fs laser pulses. Next, another bandpass dichroic mirror (DM2) is used to direct both the fs and ns laser pulses into a 36× reflective objective lens with an NA of 0.5 (Newport) providing unique specifications such as zero chromatic aberration, and negligible coma, spherical, and astigmatic aberrations. A white light is also employed for the imaging process. In order to precisely control the time delay between the laser pulses, a digital delay

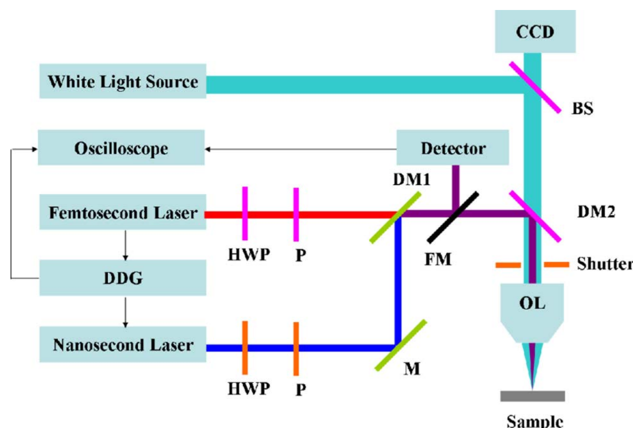

Fig. 1. (Color online) Schematic diagram of the entire fs–ns dual-beam micromachining system: HWP, half-wave plate; P, polarizer; M, mirror; FM, flipped mirror; DM, dichroic mirror; BS, beam splitter; and OL, objective lens.

0146-9592/10/142490-03$15.00/0 © 2010 Optical Society of America

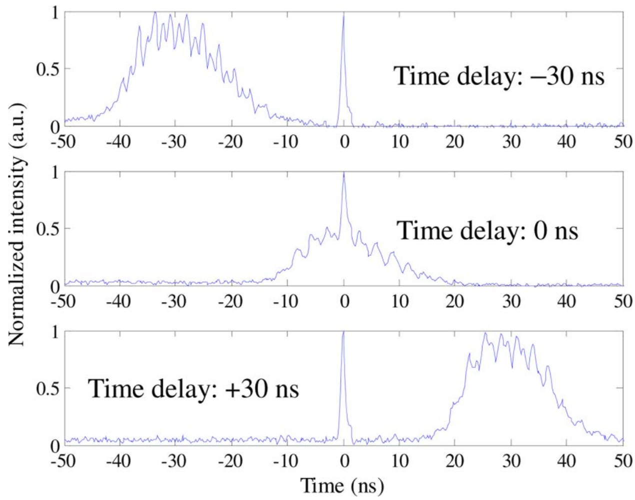

Fig. 2. (Color online) Fs–ns pulse pairs with different time delays.

generator [(DDG) DG645, Stanford Research] is employed, and the actual time delay between fs and ns pulses is monitored by a high-speed optical detector (1454, New Focus). The recorded signals from the detector, as shown in Fig. 2, in which a negative time delay is defined when the ns pulse is shot ahead of the fs pulse, and a positive time delay implies the ns pulse is shot behind the fs pulse. Note the maximum intensity shown in Fig. 2 is normalized to 1, and the relative intensity does not represent the actual pulse energy due to the optical response of the detector, which varies in the wavelength of the fs and ns laser. Because negative and positive time delays are indispensable, the nth ns laser pulse is controlled to synchronize with the $n+1$th fs laser pulse. By setting the time delay as $T \pm t_{\mathrm{delay}}$, the nth ns laser pulse can be synchronized with the $n+1$th fs pulse with $a \pm t_{\mathrm{delay}}$ time delay, where T is the repetition rate of the fs laser system and t_{delay} is the desired time delay between the fs and ns laser pulses. To enhance the repeatability of ablation results, five fs–ns pulse pairs, instead of a single fs–ns pulse pair, were selected by controlling a shutter from a steady flow of pulses continuously emitted from the lasers at a repetition rate of 10 Hz. Compared with the single-shot mode, the continuous pulsing mode provides more stable laser conditions in each laser pulse. The cleaned fused silica sample was machined by five 120 fs pulses alone (case 1), five 30 ns pulses alone (case 2), and five fs–ns pulse pairs with different time delays including −60 ns (case 3), −30 ns (case 4), 0 ns (case 5), +30 ns (case 6), and +60 ns (case 7). The machined samples were cut, and the cross-sectional images were obtained via a focused ion beam (Helios NanoLab 600, FEI).

The energies of the fs pulse and the ns pulse were adjusted as 0.12 μJ and 0.16 μJ, which, respectively, indicate the fluence of 3.8 J/cm^2 and 5.6 J/cm^2. The fluence of the ns laser is below the damage threshold of fused silica [13]. Before the sample was cut, a platinum thin film was locally coated above the machined holes to prevent unwanted damages that might be caused by the high-energy focused ions during the cutting process. All cross sections were cut through the centers of the holes. Extra care has been exercised to assure the repeatability of the experimental results. More than six experimental sets were conducted, and the results are very consistent. However, only one set of the results is presented here. Figure 3 shows the cross-sectional images of the holes machined in different cases. In Fig. 3(a) (five 120 fs pulses alone), a shallow hole was machined. The depth and the removed material volume are about 0.17 μm and 0.09 μm^3, respectively. For case 2 (five 30 ns pulses alone), Fig. 3(b) shows no apparent damage, which is due to the low absorption of the 355 nm wavelength and the wide bandgap of fused silica. Similar hole profiles and material removals to those in Fig. 3(a) are observed in −60 ns time delay, case 3 [Fig. 3(c)] and +60 ns time delay, case 7 [Fig. 3(g)] due to nonoverlapping between the fs and ns pulses. In other words, the fs and ns pulses can be considered to be independent from each other, and the ablation in each of the aforementioned cases is caused mainly by the fs pulses. In contrast, significant enhancement of material removals are observed in the cases of pulse pairs that have temporal overlapping, including −30 ns time delay [Fig. 3(d)], 0 ns [Fig. 3(e)], and +30 ns time delay [Fig. 3(f)] cases, especially in the 0 ns time delay case, in which the fs laser pulse was shot at

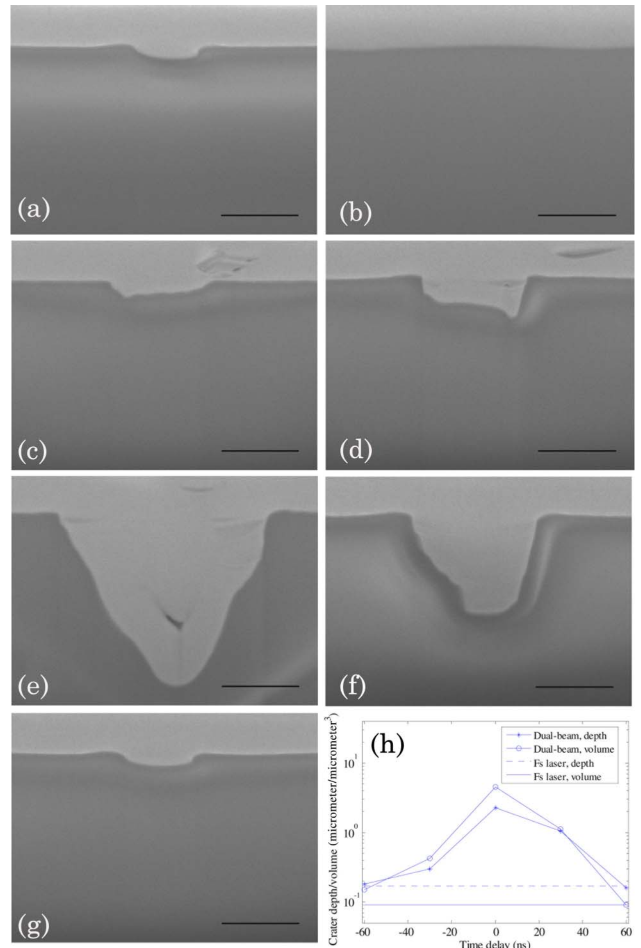

Fig. 3. (Color online) Cross-sectional images of the holes machined by (a) five 120 fs pulses, (b) five 30 ns pulses, (c) five fs–ns pulse pairs with −60 ns time delay, (d) five fs–ns pulse pairs with −30 ns time delay, (e) five fs–ns pulse pairs with 0 ns time delay, (f) five fs–ns pulse pairs with +30 ns time delay, (g) five fs–ns pulse pairs with +60 ns time delay, and (h) summary of the experimental results. The scale bar is 1 μm.

the instant of peak intensity of the ns pulse profile. For the case with 0 ns time delay between the fs and ns pulses, the depth and the removed material volume of the hole increase to about 2.28 μm and 4.56 μm^3, respectively. Compared to case 1, fs pulses alone [Fig. 3(a)] with case 5, 0 ns time delay [Fig. 3(e)], the hole depth increases from 0.17 μm to 2.28 μm and the material removal volume increases from 0.09 μm^3 to 4.56 μm^3, which correspond to the enhancement of 13.4 times in depth and 50.7 in material removal volume. Note that if the fluence of the fs laser pulse is adjusted to 2.5 J/cm^2, which is below the ablation threshold of fused silica, no ablation occurs in all cases (results not shown) even the fluence of the ns laser is increased to 6.9 J/cm^2 for the same total energy of 9.4 J/cm^2. The experiments were repeated six times, and the standard deviations in depth were less than 10% in case 1, case 3, and case 7 and less than 16% for cases 4 through 6. The summary relationships between the fs–ns time delay and the ablation depth and amount of material removal are shown in Fig. 3(h).

Recent studies have indicated that when fs laser fluences exceed the threshold ($\sim$3.3 J/cm^2 for fused silica), the critical free electron density (about 1.83×10^{21} cm^{-3}) in the fused silica is created and the fused silica possesses metallic characteristics [13,14]. Also, at the critical electron density, both the reflectivity and absorption coefficient of the fused silica increase rapidly from nearly zero in the initial stage to the values comparable to a metal [14]. Hence, when the fused silica possesses metallic characteristics, it can effectively absorb the ns laser energy, which is similar to all metals. The ns laser energy absorption in case 4 (−30 ns time delay) and case 6 (+30 ns time delay) should be very close to each other due to the symmetric locations of the ns laser pulse envelope, at which the fs laser pulse is imposed. However, in case 6 a tiny crater has already been created at the surface of the fused silica ahead of the subsequent ns pulse, which increases the absorption of the ns laser energy. Hence, in case 6, more ns laser energy is absorbed as compared to case 4. Furthermore, the subsequent energy from the ns laser pulse after the fs laser pulse may extend the lifetime of the generated free electrons in the fused silica, which enhances the material removal rate.

In summary, an enhancement of ablation efficiency has been demonstrated by a fs–ns dual-beam laser processing technique. By irradiating the fs–ns pulse pairs on the sample surface with a temporal overlapping, the metallic properties of fused silica were created due to the high free electron density generated by the fs laser pulses, which leads to the increased absorption of the subsequent ns laser energy. Hence, the change of optical properties by the fs laser pulse is the fundamental reason of a more efficient material removal of dielectrics. For the process conditions used in the present study, it is found that the fs–ns dual-beam system can increase up to 13.4 times in ablation depth and 50.7 times in the amount of material removal, as compared to fs laser ablation alone. Note the total energy of the fs–ns dual-beam system is higher than that of the fs laser alone.

This work was partially supported by the Laser Application Technology Center; the ITRI South; the Industrial Technology Research Institute, Taiwan; and the National Natural Science Foundation of China (NSFC) under grant 90923039.

References

1. D. Du, X. Liu, G. Korn, J. Squier, and G. Mourou, Appl. Phys. Lett. **64**, 3071 (1994).
2. P. P. Pronko, S. K. Dutta, J. Squier, J. V. Rudd, D. Du, and G. Mourou, Opt. Commun. **114**, 106 (1995).
3. R. R. Gattass and E. Mazur, Nature Photon. **2**, 219 (2008).
4. L. Jiang and H. L. Tsai, Appl. Phys. Lett. **87**, 151104 (2005).
5. M. Lenzner, J. Krüger, S. Sartania, Z. Cheng, C. Spielmann, G. Mourou, W. Kautek, and F. Krausz, Phys. Rev. Lett. **80**, 4076 (1998).
6. L. Jiang and H. L. Tsai, ASME J. Heat Transfer **127**, 1167 (2005).
7. B. Rethfeld, A. Kaiser, M. Vicanek, and G. Simon, Phys. Rev. B **65**, 214303 (2002).
8. K. Sugioka, S. Wada, H. Tashiro, K. Toyoda, Y. Ohnuma, and A. Nakamura, Appl. Phys. Lett. **67**, 2789 (1995).
9. J. Zhang, K. Sugioka, T. Takahashi, K. Toyoda, and K. Midorikawa, Appl. Phys. A **71**, 23 (2000).
10. Y. P. Deng, X. H. Xie, H. Xiong, Y. X. Leng, C. F. Cheng, H. H. Lu, R. X. Li, and Z. Z. Xu, Opt. Express **13**, 3096 (2005).
11. M. Li, S. Menon, J. P. Nibarger, and G. N. Gibson, Phys. Rev. Lett. **82**, 2394 (1999).
12. A. C. Forsman, P. S. Banks, M. D. Perry, E. M. Campbell, A. L. Dodell, and M. S. Armas, J. Appl. Phys. **98**, 033302 (2005).
13. B. C. Stuart, M. D. Feit, A. M. Rubenchik, B. W. Shore, and M. D. Perry, Phys. Rev. Lett. **74**, 2248 (1995).
14. L. Jiang and H. L. Tsai, Int. J. Heat Mass Transfer **48**, 487 (2005).